Dimers of mitochondrial ATP synthase form the permeability transition pore

Valentina Giorgio[a], Sophia von Stockum[a], Manuela Antoniel[b], Astrid Fabbro[b], Federico Fogolari[c], Michael Forte[d], Gary D. Glick[e], Valeria Petronilli[a], Mario Zoratti[a], Ildikó Szabó[f], Giovanna Lippe[b,1], and Paolo Bernardi[a,1]

[a]Consiglio Nazionale delle Ricerche Institute of Neuroscience and Department of Biomedical Sciences and [f]Department of Biology, University of Padova, 35121 Padua, Italy; Departments of [b]Food Science and [c]Medical and Biological Sciences, University of Udine, 33100 Udine, Italy; [d]Vollum Institute, Oregon Health and Sciences University, Portland, OR 97239; and [e]Department of Chemistry, Graduate Program in Immunology, University of Michigan, Ann Arbor, MI 48109

Edited* by Tullio Pozzan, Foundation for Advanced Biomedical Research, Padua, Italy, and approved March 4, 2013 (received for review October 12, 2012)

Here we define the molecular nature of the mitochondrial permeability transition pore (PTP), a key effector of cell death. The PTP is regulated by matrix cyclophilin D (CyPD), which also binds the lateral stalk of the F_OF_1 ATP synthase. We show that CyPD binds the oligomycin sensitivity-conferring protein subunit of the enzyme at the same site as the ATP synthase inhibitor benzodiazepine 423 (Bz-423), that Bz-423 sensitizes the PTP to Ca^{2+} like CyPD itself, and that decreasing oligomycin sensitivity-conferring protein expression by RNAi increases the sensitivity of the PTP to Ca^{2+}. Purified dimers of the ATP synthase, which did not contain voltage-dependent anion channel or adenine nucleotide translocator, were reconstituted into lipid bilayers. In the presence of Ca^{2+}, addition of Bz-423 triggered opening of a channel with currents that were typical of the mitochondrial megachannel, which is the PTP electrophysiological equivalent. Channel openings were inhibited by the ATP synthase inhibitor AMP-PNP (γ-imino ATP, a nonhydrolyzable ATP analog) and Mg^{2+}/ADP. These results indicate that the PTP forms from dimers of the ATP synthase.

The permeability transition (PT) defines an increased permeability of the inner mitochondrial membrane to ions and solutes triggered by matrix Ca^{2+} in the presence of specific inducers, the most classical being Pi and thiol oxidants (1). The sensitivity to Ca^{2+} is decreased by several compounds, including Mg^{2+}, adenine nucleotides, and cyclosporin A (CsA) (2). In vitro at least, the PT is accompanied by swelling of mitochondria, which has long been known to prevent ATP synthesis (3). The idea that swelling could be mediated by a Ca^{2+}-regulated pore was advanced in the 1970s (4, 5), and its basic regulatory features were defined in a series of seminal studies in 1979 (6–8). The PT is mediated by opening of a high-conductance channel, the PT pore (PTP), which was identified by patch-clamping of the inner membrane and called mitochondrial megachannel (MMC) (9–12). Opening of the PTP is causally involved in cell death associated with many diseases, including heart ischemia (13), and its role is particularly well-documented in muscular dystrophy caused by defects of collagen VI (14). The molecular nature of the channel(s) involved remains a mystery. The long-standing idea that the PTP forms at contact sites of the inner and outer membranes through voltage-dependent anion channel (VDAC) and the adenine nucleotide translocator (ANT) (15) proved incorrect, because VDAC- and ANT-null mitochondria still display a CsA-sensitive PT (16–18).

A well-characterized protein regulator of the PTP is cyclophilin D (CyPD), which in the mouse is encoded by the *Ppif* gene. CyPD sensitizes the PTP to Ca^{2+}, as deduced from experiments in mitochondria from *Ppif*$^{-/-}$ mice where the PT required higher loads of matrix Ca^{2+} (19–22), a behavior that is perfectly matched by the MMC (23). CyPD binds the F_OF_1 ATP synthase (complex V), the rotary enzyme that synthesizes the vast majority of ATP in respiring cells (24). This complex is formed by the catalytic F_1, the membrane-bound proton-translocating F_O, and a lateral stalk linking F_1 and F_O. CyPD binds the lateral stalk, which acts as a stator to counter the tendency of the $\alpha_3\beta_3$-subcomplex of the F_1-catalytic domain to rotate with the rotor containing the F_1 subunits-γ, -δ, and -ε and a ring of F_O subunits c (25). CyPD binding requires Pi and results in partial inhibition of ATP synthase activity, whereas CsA displaces CyPD, resulting in enzyme reactivation (24). Despite the striking analogy with PTP regulation, whether these interactions are relevant for the PT remains unknown. Here, we show that dimers of the F_OF_1 ATP synthase incorporated into lipid bilayers form Ca^{2+}-activated channels with the key features of the MMC-PTP (10–12).

Results

CyPD Binds Oligomycin Sensitivity-Conferring Protein Subunit of ATP Synthase. We identified potential binding site(s) of CyPD to the F_OF_1 ATP synthase in the b, d, and oligomycin sensitivity-conferring protein (OSCP) subunits of the lateral stalk (24). To more precisely define the specific partner(s) of CyPD within this complex, we devised conditions optimizing its binding to the ATP synthase, while separating the subunits of the peripheral stalk. The first condition was met by using 10 mM Pi and low ionic strength (24); the second condition was met by adding a low concentration of SDS to the Triton X-100–based extraction buffer and using a polyclonal antibody against a peptide mapping near the C terminus of OSCP, which disrupts the interaction of the OSCP C-terminal domain with the N-terminal portion of subunit b (25). This strategy allowed the immunoprecipitation of individual OSCP, b, and d subunits, because no other stalk protein was detected in the specific immunoblots (Fig. 1*A*). CyPD was found exclusively in the immunoprecipitation with OSCP antibody, suggesting that OSCP is the direct interactor of CyPD in the ATPase complex (Fig. 1*A*). We next used OSCP-specific siRNAs in HQB17 cells (26), where we studied the expression of selected ATP synthase subunits in total extracts of mitochondria. We found the expected decrease of OSCP, but not of F_1 α- and β- subunits or CyPD (Fig. 1*B*, *Left*). When the ATP synthase was immunoprecipitated from mitochondria with decreased levels of OSCP, decreased levels of CyPD were detected as well, which precisely matched the decreased association of OSCP to the enzyme complex (Fig. 1*B*, *Right*). It should be noted that cells with stably reduced OSCP levels do not display decreased levels of α-, β-, and d subunits or alterations of mitochondrial membrane potential or mitochondrial ultrastructure, indicating that assembly and function of ATP synthase are not compromised (27).

Author contributions: V.G., S.v.S., F.F., M.Z., I.S., G.L., and P.B. designed research; V.G., S.v.S., M.A., A.F., F.F., and I.S. performed research; M.F. and G.D.G. contributed new reagents/analytic tools; V.G., F.F., M.F., G.D.G., V.P., M.Z., I.S., G.L., and P.B. analyzed data; and G.L. and P.B. wrote the paper.

Conflict of interest statement: Bz-423 is licensed to a company in which G.D.G. has ownership interest and receives compensation.

*This Direct Submission article had a prearranged editor.

[1]To whom correspondence may be addressed. E-mail: giovanna.lippe@uniud.it or bernardi@bio.unipd.it.

This article contains supporting information online at www.pnas.org/lookup/suppl/doi:10.1073/pnas.1217823110/-/DCSupplemental.

BIOCHEMISTRY

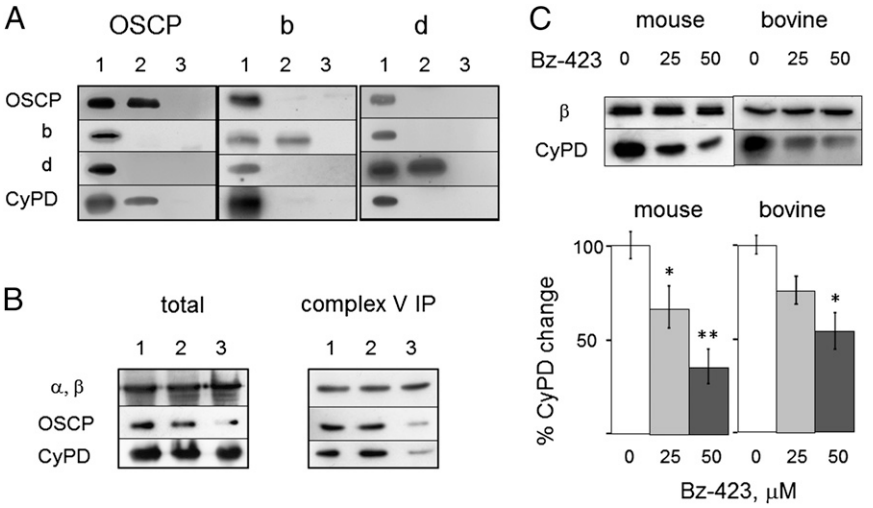

Fig. 1. CyPD interacts with OSCP and is displaced by Bz-423. (*A*) Extracts and immunoprecipitates of BHM with anti-OSCP or b or d subunit antibodies were immunoblotted as indicated. Lane 1, mitochondria; lane 2, immunoprecipitates with OSCP (*Left*), b (*Center*), and d (*Right*) antibodies; lanes 3, IgG antibody. (*B*) Total cell extracts (*Left*) and complex V immunoprecipitates (*Right*) of mitochondria from cells either untreated (lane 1) or treated with scrambled siRNA (lane 2) or OSCP siRNA (lane 3) probed for F_1 α,β-subunits, OSCP, and CyPD. (*C*) Heart mitochondria were treated with the indicated concentrations of Bz-423 (μM), immunoprecipitated with anticomplex V antibodies, and immunoblotted with antibodies against β-subunit or CyPD. Ratio between CyPD and β-band intensities is reported ($n = 3 \pm$ SE). $^*P \leq 0.02$; $^{**}P = 0.0015$, Student *t* test.

CyPD–OSCP interactions were mostly electrostatic in nature, because they could be disrupted by increased ionic strength (Fig. S1*A*). A study of surface potentials and isopotential curves of CyPD and OSCP in the ATP synthase complex (Fig. S1 *B* and *C*) identified putative binding regions of CyPD on OSCP at the residues indicated in Fig. S1*C*. This region overlaps with helices 3 and 4, the binding site of benzodiazepine 423 (Bz-423), a well-characterized inhibitor of the F_OF_1 ATP synthase that readily permeates mitochondria (27, 28). We, therefore, tested the effect of Bz-423 on the association of CyPD to mouse and bovine complex V at 10 mM Pi, and we found a concentration-dependent displacement that is consistent with competition for a common binding site (Fig. 1*C*). This set of experiments documents that OSCP is the partner of CyPD on the lateral stalk, that no CyPD binding occurs in the absence of OSCP, and that the binding site covers the same region where Bz-423 binds the OSCP subunit.

Bz-423 Induces the PTP. To test whether the interaction of Bz-423 with OSCP is also relevant for PTP modulation, we studied the Ca^{2+} retention capacity (CRC) of mitochondria allowing the definition of the threshold matrix Ca^{2+} load required to trigger pore opening. Bz-423 decreased the CRC of mitochondria at 1 mM Pi but not 5 mM Pi (Fig. 2*A*). In the presence of CsA (Fig. 2*B*), which displaces CyPD from OSCP (24), or in CyPD-null mitochondria (Fig. 2*C*), the PTP-sensitizing effect of Bz-423 was observed at 5 mM Pi as well. This behavior matched the inhibitory profile of Bz-423 on ATP hydrolysis, which required higher concentrations of Bz-423 only in CyPD-competent mitochondria at high Pi concentrations (Fig. S2). Inhibition of ATP synthase with resveratrol (29) and oligomycin was instead independent of CyPD (Fig. S3). These results highlight a striking analogy between the effects of Bz-423 on PTP and ATP synthase.

ATP Synthase Activity and OSCP Affect the PTP. Adenine nucleotides are inhibitors of the PT (6), but their mechanism of action is unknown. We explored the hypothesis that nucleotides affect the Ca^{2+} sensitivity of the PTP through the catalytic activity of the F_OF_1 ATP synthase. We incubated mitochondria either (*i*) with ADP and respiratory substrates in the presence of an ATP-hydrolyzing system based on hexokinase plus glucose (so that mitochondria were energized by the respiratory chain, the ADP concentration was constant, and rotation of the ATP synthase was clockwise when viewed from the membrane side) (30) or (*ii*) with ATP in the presence of an ATP-regenerating system based on phosphocreatine and creatine kinase in the absence of substrates (so that mitochondria were energized by ATP hydrolysis at constant levels of ATP, and rotation of the ATP synthase was in the opposite direction) (30). In either case, mitochondria developed a membrane potential as shown by accumulation of Rhodamine 123 (Fig. 3*A*), which responded appropriately to the addition of oligomycin [i.e., with hyperpolarization in ATP-synthesizing mitochondria (Fig. 3*A*, trace a) and depolarization in ATP-hydrolyzing mitochondria (Fig. 3*A*, trace b)] and the uncoupler carbonylcyanide-*p*-trifluoromethoxyphenyl hydrazone. PTP opening in ATP-hydrolyzing mitochondria (constant ATP levels) required two times the Ca^{2+} load of ATP-synthesizing mitochondria (constant ADP levels) (Fig. 3*B*). The mean ratio between ATP-hydrolyzing and -synthesizing mitochondria was 2.06 ± 0.27 in four independent experiments per condition, an effect that matches the effect of CsA in mouse liver mitochondria (20). This difference was not due to the nucleotides per se,

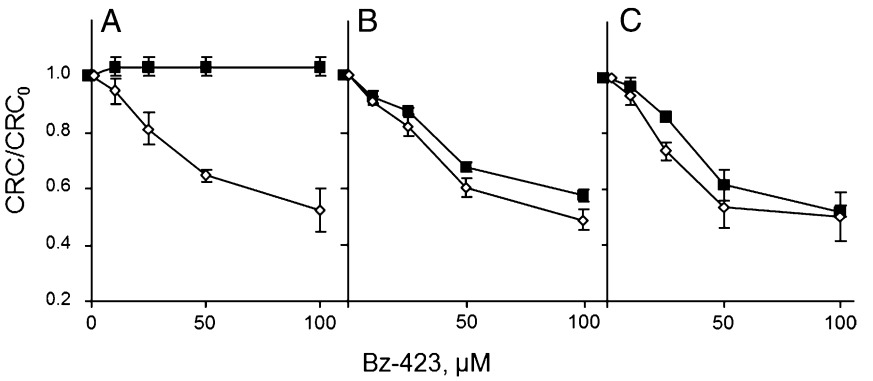

Fig. 2. Bz-423 decreases the mitochondrial Ca^{2+} retention capacity. Isolated WT (*A* and *B*) or *Ppif*$^{-/-}$ mouse liver mitochondria (*C*) were incubated in the presence of 1 (open symbols) or 5 mM (closed symbols) Pi·Tris and Bz-423 as indicated. In *B* only, 1.6 μM CsA was added. Extramitochondrial Ca^{2+} was monitored, and CRC was determined by stepwise addition of 10 μM Ca^{2+} pulses. The measured CRC (i.e., the amount of Ca^{2+} accumulated before onset of Ca^{2+}-induced Ca^{2+} release) was normalized to that obtained in absence of Bz-423 (CRC_0), and data are average of triplicate experiments ± SE. Absolute CRC values (nmol Ca^{2+}/mg protein) at 1 mM Pi were 120 ± 0, 160 ± 20, and 166.7 ± 30.6 for *A*, *B*, and *C*, respectively; absolute CRC values (nmol Ca^{2+}/mg protein) at 5 mM Pi were 86.7 ± 11.5, 126.7 ± 30.6, and 160 ± 20 for *A*, *B*, and *C*, respectively ($n = 3 \pm$ SD).

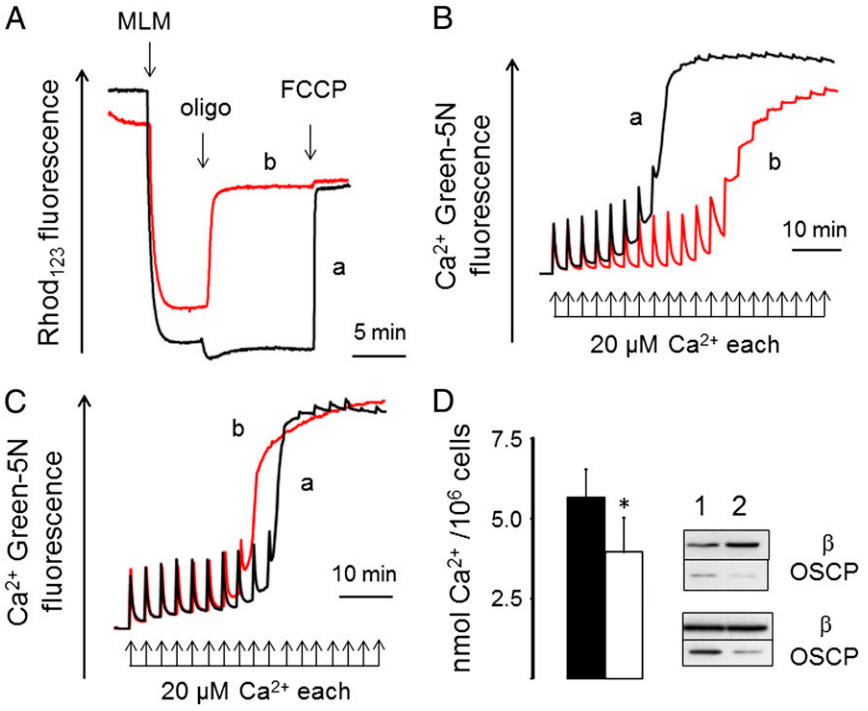

Fig. 3. ATP synthase catalysis and OSCP knockdown affect the Ca^{2+} sensitivity of the PT. (*A*) Membrane potential was measured in mitochondria incubated with respiratory substrate and ADP plus an ATP-consuming system (trace a) or no substrate, ATP, and an ATP-regenerating system (trace b) as detailed in *Materials and Methods*. Where indicated, 2 mg mouse liver mitochondria (MLM), 1 μg/mL oligomycin (oligo), and 1 μM carbonylcyanide-*p*-trifluoromethoxyphenyl hydrazone (FCCP). (*B*) Conditions for traces a and b were exactly as in *A*, but Ca^{2+} was measured. (*C*) The incubation medium contained respiratory substrate and 1 μg/mL oligomycin, and it was supplemented with 0.4 mM ADP (trace a) or 0.4 mM ATP (trace b); one experiment representative of three is shown. (*D*) Scrambled siRNA- or OSCP siRNA-treated cells (closed and open bars, respectively) were permeabilized with digitonin, and their CRC was measured in the presence of an ATP-regenerating system. Data are average ± SD of nine independent determinations per condition. $*P = 0.0025$ (Student *t* test). The blots display the levels of OSCP and F_1 β-subunits in the two batches of cells used (lanes 1, scrambled siRNA; lanes 2, OSCP siRNA).

because in the presence of oligomycin ADP was actually slightly more effective than ATP (Fig. 3*C*, traces a and b, respectively). We could exclude any contribution from endoplasmic reticulum contaminants, because no Ca^{2+} uptake was seen in the presence of ATP plus oligomycin (Fig. S4). These results indicate that the catalytic activity of ATP synthase (synthesis vs. hydrolysis) affects the Ca^{2+} sensitivity of the PTP.

We also tested the effect of OSCP knockdown on the sensitivity of the PTP to Ca^{2+} in permeabilized HQB17 cells using ATP hydrolysis to generate the proton gradient. Lowered OSCP expression decreased the threshold Ca^{2+} required for opening (Fig. 3*D*). It should be noted that OSCP-depleted mitochondria did take up a sizeable amount of Ca^{2+} before onset of the PT (Fig. 3*D*), consistent with a conserved catalytic activity of ATP synthase and the buildup of the proton gradient (27). Thus, lack of the stalk subunit OSCP increases the Ca^{2+} sensitivity of the PTP, suggesting that the F_OF_1 ATP synthase is involved in its formation. This hypothesis was tested in ATP synthase preparations.

Purified ATP Synthase Dimers Have PTP Channel Activity. We separated mitochondrial proteins by blue native electrophoresis (BNE) (31) and identified the ATP synthase by in-gel activity (Fig. 4*A*). SDS/PAGE of dimers and monomers eluted from BNE gels (Fig. 4*B*) displayed the same subunit pattern previously shown in high-resolution gels (32). Western blotting detected the occasional presence of some respiratory complexes I and III in the dimers (the I + III supercomplex runs very close to complex V dimers in BNE) but not VDAC, CyPD, or ANT (Fig. 4*C*), which in BNE with digitonin migrates with the electrophoretic front as an individual protein (31).

The gel-purified ATP synthase dimers or monomers were incorporated in planar lipid bilayers. Addition of Bz-423 to the dimer in the presence of Ca^{2+} elicited channel activity, whereas no such activity was observed when the drug was added to the monomer (Fig. 5*A*). Addition of phenylarsine oxide (PhAsO), one of the most powerful sensitizers of the PTP to Ca^{2+} (1), was not sufficient to induce channel opening, but the subsequent addition of Bz-423 induced activity with similar characteristics to Bz-423 alone (Fig. 5*B* and Fig. S5). Moreover, γ-imino ATP (AMP-PNP), a nonhydrolyzable ATP analog (33), inhibited current conduction even in the presence of PhAsO (Fig. 5*B*). The characteristics of the pore closely matched the features of MMC-PTP (10–12): the maximal chord conductance was 1.0–1.3 nS in 150 mM KCl, and various subconductance states were commonly entered (Fig. 5 *C* and *D*). Transitions of about 1.0 and 0.5 nS, typical of MMC-PTP activity, are shown in Fig. S6*A*. Again in keeping with the properties of MMC, the activity could be largely inhibited by Mg^{2+} and nearly completely inhibited by Mg^{2+} plus ADP (Fig. 5*C*); however, it could not be inhibited by CsA, like the MMC of *Ppif*$^{-/-}$ mitochondria (23), coherently with the lack of CyPD in the preparation (Fig. 4*C*). Other inducers beside Pi and Ca^{2+} were not strictly necessary to induce PTP currents, as shown in Fig. S6*B*, where Ca^{2+} was added at 3 mM and the ATP synthase dimer was extracted in the presence of 10 mM Pi, which sensitizes the PTP even in the absence of CyPD (1).

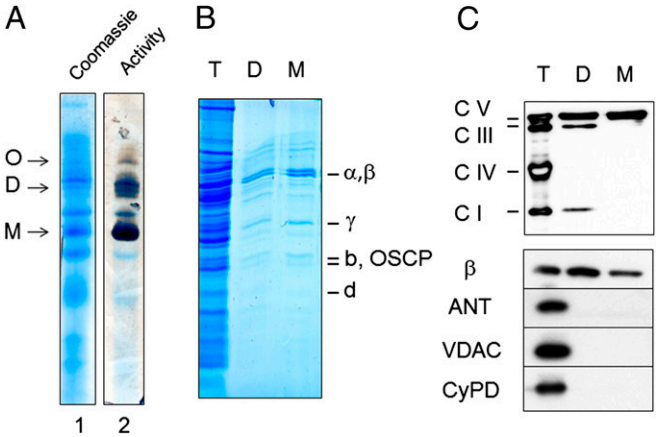

Fig. 4. Purification of F_OF_1 ATP synthase. (*A*) BHM were subjected to BNE to separate oligomers (O), dimers (D), and monomers (M) of ATP synthase, which were identified by Coomassie blue (lane 1) and in-gel activity staining (lane 2). Dimers and monomers were excised, eluted, subjected to SDS/PAGE, and stained with colloidal Coomassie (*B*), or they were transferred to nitrocellulose and tested for respiratory complexes and ATP synthase, subunit-β of F_1, ANT, VDAC, and CyPD (*C*). T, D, and M refer to total extract, dimer, and monomer, respectively. One experiment representative of three is shown.

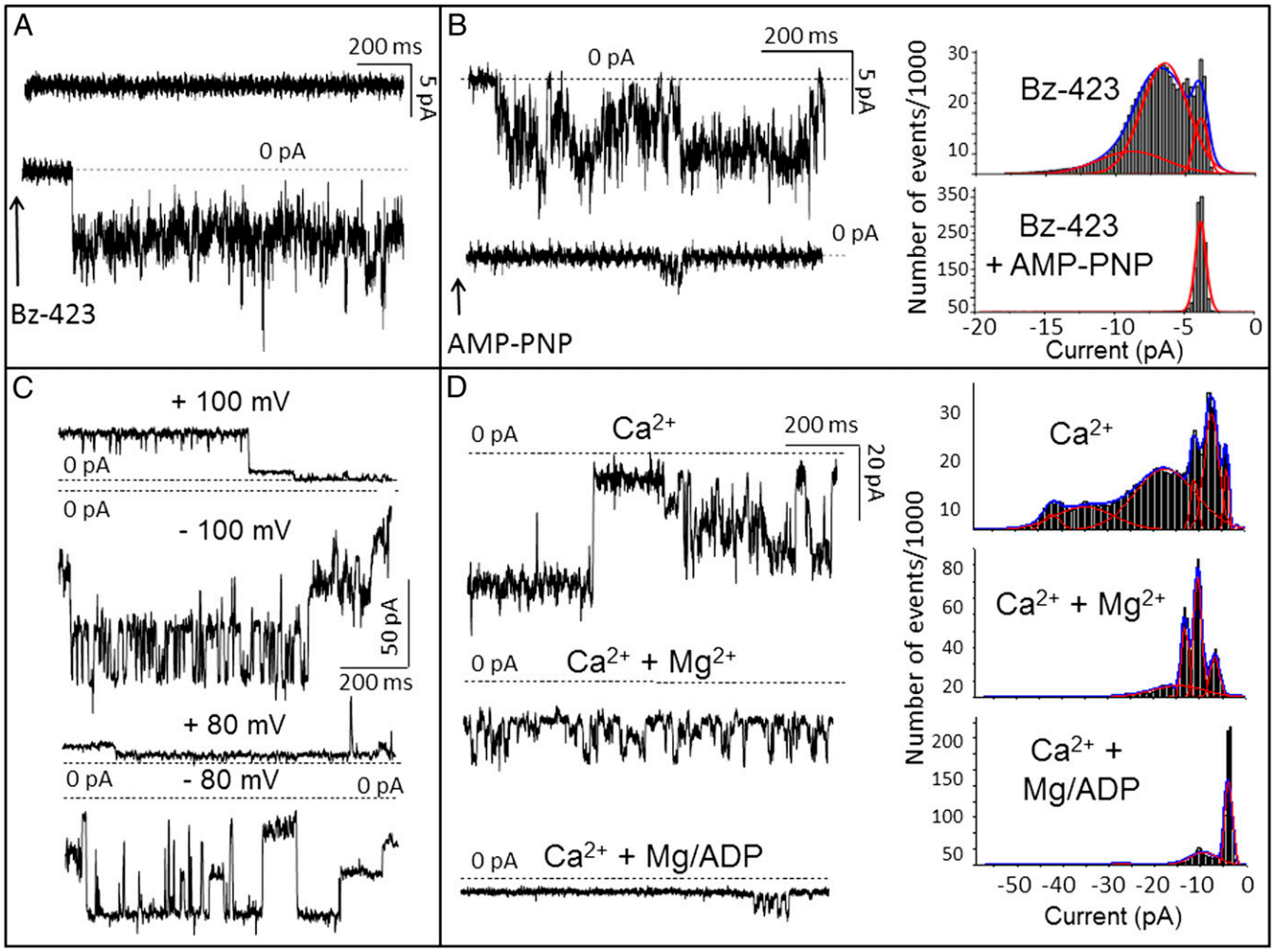

Fig. 5. Dimers of F_OF_1 ATP synthase generate currents matching MMC-PTP. (*A*) A bilayer experiment in 50 mM KCl, 1 mM Pi, and 0.3 mM Ca^{2+} (Ca^{2+} only *in trans*; $V_{cis} = -60$ mV). After addition of dimeric ATP synthase, no activity could be observed (*Upper*) until immediately after the addition of 0.1 mM Bz-423 to the *trans* side (*Lower*; arrow). When monomers were used, the recording was identical to *Upper*, which was not modified by the addition of Bz-423. (*B*) A similar experiment in the presence of 0.1 mM PhAsO *in trans*. Activity (*Upper*) was elicited by the addition of Bz-423 as in *A* and inhibited by 0.1 mM AMP-PNP in *trans* (*Lower*; arrow). Corresponding current amplitude histograms from gap-free 60-s traces are shown in *Right*. (*C*) Current traces (150 mM KCl; V_{cis} as indicated) with dimeric ATP synthase and 0.3 mM Ca^{2+}, 0.1 mM Bz-423, and 50 μM PhAsO added to the *trans* side. Note numerous substates. (*D*, *Left*) Activity ($V_{cis} = -80$ mV) recorded as in *C* (first trace) and after sequential additions of Mg^{2+} (0.6 mM) and ADP (0.6 mM) to the *trans* side; (*D*, *Right*) corresponding amplitude histograms from gap-free 100-s traces. Representative experiments are shown of a total of 28 experiments performed under various conditions using six different ATP synthase dimer preparations.

Channel openings were still observed in the presence of bongkrekic acid and could not be elicited by atractyloside, selective inhibitors of ANT. Rather, in some cases, atractyloside induced a small conductance (Fig. S7). Of note, channels were not observed with gel-purified complex I, indicating that this occasional contaminant also cannot be responsible for the current that we observe in the purified dimers of F_OF_1 ATP synthase (Fig. S7). The ATP synthase preparations still possessed enzymatic activity after extraction from the gels for incorporation in the bilayers, which was shown by a second BNE and activity staining (Fig. S8).

Discussion

We have shown that CyPD interacts with the ATP synthase at OSCP subunit. This observation, which builds on our previous work on regulation of the ATP synthase by CyPD (24), led to identification of the elusive PTP as a dimer of the F_OF_1 ATP synthase. The electrophysiological features displayed by our ATP synthase preparation are very different from the currents of the ANT, which has been proposed to take part in PTP formation (15) and is still included in models of the PTP in association with the Pi carrier (34). The ANT exhibits a conductance ranging between 50 and 700 pS in 100 mM KCl (35), which is lower than the currents displayed by the MMC (9–12); it shows low probability of current fluctuation at voltages lower than 150 mV at variance from the reconstituted ATP synthase dimers (Fig. 5), and it can be inhibited only by ADP and bongkrekic acid together, whereas ADP alone had a marginal effect (35–37). Patch-clamp experiments with the reconstituted, functionally active mitochondrial Pi carrier revealed an anion channel function with a mean conductance as low as 40 ± 10 pS, which was decreased to 25 ± 5 pS by Ca^{2+} and Mg^{2+}, inhibited by Pi, and unaffected by ADP (38). These features make the Pi carrier a very unlikely candidate as a PTP component, and they rule out that the currents observed here may be related to this protein.

Bz-423 was discovered and characterized as an apoptosis-inducing agent acting through mitochondria (39); identification of OSCP as its target was achieved through the screening of a human cDNA T7 phage display library (27) and the interaction with ATP synthase resulting in inhibition of enzyme activity confirmed by NMR (28). The striking selectivity of action of Bz-423

on OSCP and its ability to trigger channel activity of ATP synthase dimers, together with the lack of activity of monomer preparations, argues against the possibility that the currents that we observe are caused by unidentified contaminating proteins. This conclusion is strengthened by the inhibitory effect of AMP-PNP and Mg^{2+}/ADP on channel activity.

The PTP-inducing effect of Bz-423 and CyPD (which both act through OSCP on top of the lateral stalk in the matrix) is necessarily indirect, because it impinges on the permeability properties of the inner membrane. Because a current is only seen with the dimers, it is logical to conclude that the PTP forms at the membrane interface between two adjacent F_O sectors, which would be in keeping with the well-characterized effects of fatty acids and lysophospholipids on the PTP (1). The essential role of matrix Ca^{2+} in PTP formation is intriguing. Ca^{2+} is able to sustain ATP hydrolysis by complex V with a similar K_m as Mg^{2+} and to compete with Mg^{2+} for the catalytic sites (40). Interestingly and in contrast with other divalent metal–ATP complexes, the ATPase activity is not coupled to proton translocation when Ca^{2+} is bound, suggesting that Ca^{2+} induces conformational changes in F_O, which could then mediate PTP formation and explain the inability of Ca^{2+} to sustain ATP synthesis (41). As shown here, accessibility of the PTP Ca^{2+} binding sites is influenced by enzyme catalysis and OSCP. One possible explanation is that the OSCP subunit affects the affinity of the metal binding sites of ATP synthase, and thus the ease with which matrix Ca^{2+} can replace Mg^{2+}, causing PTP opening. OSCP as such would be a negative modulator, and its effect would be counteracted by binding of the positive effector CyPD (which indeed increases the Ca^{2+} affinity of the PTP). Removal of OSCP, or CyPD binding to OSCP, would induce similar conformational effects, consistent with the data presented here as well as with previous findings on CyPD interactions with the lateral stalk (24).

Although defining the detailed mechanism of PTP formation requires additional work, the demonstration that the PTP forms from dimers of the F_OF_1 ATP synthase solves a long-lasting issue in cell biology and readily accommodates key pathophysiological effectors of the PT. Indeed, Ca^{2+}, Mg^{2+}, adenine nucleotides, and Pi bind the catalytic core at F_1, and the membrane potential and matrix pH, which are key PTP modulators (1), are also key regulators of the ATP synthase. Channel formation by purified ATP synthase dimers confirms our long-standing stance that the PT is an inner membrane event that does not require outer membrane components (1), which is also in keeping with recent results that we obtained in mitoplasts (42). The present findings suggest a dual function for complex V, i.e., ATP synthesis and PTP formation. The enzyme of life seems, therefore, to be also the molecular switch that may signal the presence of fully depolarized, dysfunctional mitochondria to stimulate cell death (1) and/or mitophagy (43). The detailed mechanisms through which this transition is achieved can now be addressed with the powerful tools of genetics, and we have little doubt that clarification of the molecular determinants of PTP formation will provide the solution to outstanding problems on the role of PTP in pathophysiology.

Materials and Methods

Immunoprecipitation and Western Blotting. Immunoprecipitation (IP) of ATP synthase was performed from 0.5 mg bovine, mouse heart, or human osteosarcoma HQB17 cells mitochondria prepared by standard methods (44, 45) using anticomplex V monoclonal antibody covalently linked to protein G-Agarose beads (MS501 immunocapture kit; Abcam) as reported (24). For isolated subunits, 30 μL *Staphylococcus aureus* protein A-Sepharose 4B (Sigma) were coupled with 10 μg OSCP subunit antibody, 2 μg b subunit, or nonimmune antibody in IP buffer (15 mM Tris, 10 mM Pi·Tris, 2 mM EDTA·Tris, 1.8 mM EGTA·Tris, 0.5% vol/vol Triton X-100, 0.005% wt/vol BSA, 0.25% SDS, pH 7.4) and incubated for 2 h at 4 °C. Then, 0.5 mg bovine heart mitochondria (BHM) solubilized and precleared in IP buffer were added with protein A-coupled antibody and incubated overnight at 4 °C. For d subunit, BHM was suspended in IP buffer, incubated for 1 h at 4 °C with 4 μg anti-d or rabbit anti-mouse antibodies, and then incubated for 3 h at 4 °C with 30 μL protein A. IP supernatants were separated by SDS/PAGE followed by Western blot analysis. Antibodies were polyclonal rabbit anti-α and -β F_1 subunit, anti-b subunit (a gift from John Walker, Medical Research Council—Mitochondrial Biology Unit, Cambridge), anti-ANT Q18 (Santa Cruz Biotechnology), monoclonal anti-β, anti-d subunit, anti-OXPHOS (Mitoscience), anti-CyPD (Calbiochem), anti-OSCP (Abcam), and anti-VDAC1 (a gift from F. Thinnes, Max-Planck-Institut für Experimentelle Medizin, Abteilung Immunchemie, Göttingen, Germany). Immunoreactive bands were detected by enhanced chemiluminescence (Pierce). CyPD is expressed as CyPD/β-ratio of bands analyzed with Quantity One software (Biorad). Statistics were calculated by GrafPad software.

Transfection with siRNAs. HQB17 cells (26) were transfected with an siRNA duplex OSCP oligo ribonucleotides pool (Invitrogen) as follows: ATP5OHSS100870 (-GGA ACC CAA AGU GGC UGC UUC UGU U-, -AAC AGA AGC AGC CAC UUU GGG UUC C-), ATP5OHSS100872 (-CAG GGC UAU GCG GGA GAU UGU CUA A-, -UUA GAC AAU CUC CCG CAU AGC CCU G-), or scrambled sequence at 0.2 μM. Before treatment, cybrids were cultured without antibiotics for 24 h and then transfected with siRNA and Lipofectamine 2000 in Opti-MEM (Invitrogen). After 6 h, the medium was replaced with culture medium without siRNA for 66 h before preparation of mitochondria.

Mitochondrial CRC and Membrane Potential. Extramitochondrial Ca^{2+} was measured by Calcium Green-5N (Molecular Probes) fluorescence (46) using a Fluoroskan Ascent FL (Thermo Electron) plate reader at a mitochondrial concentration of 1 mg × mL^{-1}. Membrane potential was measured at 25 °C using a Perkin-Elmer LS50B spectrofluorometer based on the fluorescence quenching of 0.15 μM Rhodamine 123 (46). For measurements of CRC and membrane potential during ATP synthesis at constant [ADP] (Fig. 3 *A*, trace a and *B*, trace a), the incubation medium contained 0.1 M glucose, 80 mM KCl, 10 mM Mops·Tris, 5 mM succinate·Tris, 4 mM $MgCl_2$, 1 mM Pi·Tris, 0.5 mM $NADP^+$, 0. 4 mM ADP, 50 μM P1,P5-di(adenosine-5′) pentaphosphate, 10 μM EGTA, 2 μM rotenone, 4 U/mL glucose-6-phosphate dehydrogenase, and 3 U/mL hexokinase. We ascertained that mitochondrial respiration was maximally stimulated and that the added enzymes were in excess by measuring O_2 consumption with a Clark oxygen electrode. For measurements of CRC and membrane potential during ATP hydrolysis at constant [ATP] (Fig. 3 *A*, trace b and *B*, trace b), the incubation medium contained 0.1 M sucrose, 80 mM KCl, 10 mM Mops·Tris, 4 mM $MgCl_2$, 2 mM phosphocreatine, 1 mM Pi·Tris, 0.4 mM ATP, 10 μM EGTA, 2 μM rotenone, and 1.5 U/mL creatine kinase. We ascertained that the ATP-regenerating activity was in excess by measuring the mitochondrial membrane potential, which was sustained at the maximal value beyond the duration of the CRC experiments. For all other CRC measurements (Figs. 2 and 3*C* and Fig. S4), the incubation medium contained 0.1 M sucrose, 80 mM KCl, 10 mM Mops·Tris, 5 mM succinate·Tris, 4 mM $MgCl_2$, 1 mM Pi·Tris, 10 μM EGTA·Tris, 2 μM rotenone, 0.5 μM Ca^{2+} Green-5N, and 1 mg/mL mitochondria. Additional modifications or additions are specified. Measurements of ATP hydrolysis were performed according to published methods (47, 48).

BNE Gel and Sample Preparation for Electrophysiology. Pellets of mitochondria were suspended at 10 mg/mL in 1 M aminocaproic acid and 50 mM Bis·Tris, pH 7.0 (24), solubilized with 2% (wt/vol) digitonin, and immediately centrifuged at 100,000 × *g* for 25 min at 4 °C. The supernatants were supplemented with Coomassie Blue G-250 (Serva) and rapidly applied to 1D 4–11% polyacrylamide gradient BNE (Invitrogen). After electrophoresis, gels were stained with Coomassie Blue, used for in-gel activity staining, or prepared for an overnight native complex protein elution from BNE gel as follows. Bands corresponding to monomers and dimers of complex V or monomer of complex I were excised and diluted with 25 mM tricine, 7.5 mM Bis·Tris, and 1% (wt/vol) n-heptyl β-D-thioglucopyranoside, pH 7.0 (49) supplemented with 8 mM ATP·Tris and 10 mM $MgSO_4$. After overnight incubation at 4 °C, samples were centrifuged at 20,000 × *g* for 10 min at 4 °C, and supernatants were (*i*) used directly for reconstitution in electrophysiological studies, (*ii*) subjected to 2D-SDS PAGE separation followed by Western blotting, or (*iii*) loaded in 2D-BNE followed by Coomassie Blue or in-gel activity staining (ATPase activity was amplified as in ref. 50).

Electrophysiology. Planar lipid bilayer experiments were performed as described (51). Briefly, bilayers of about 150–200 pF capacity were prepared using purified soybean azolectin. The standard experimental medium was 150 mM KCl and 10 mM Hepes, pH 7.4. Control experiments with empty membrane or detergents used for the purification showed no activity. All voltages reported refer to the *cis* chamber, zero being assigned by convention to the *trans* (grounded) side. Currents are considered as positive when carried by cations flowing from the *cis* to the *trans* compartment. Data were acquired at 100 μs/point, filtered at 500 Hz, and analyzed offline using the pClamp program set (Axon Instruments). Histograms were fitted using the Origin7.5 program set.

Electrostatic Calculations. The molecular structures of the membrane extrinsic region of the bovine ATP synthase (Protein Data Bank ID code 2WSS, chains) (25) and human CyPD complexed with CsA (Protein Data Bank ID code 2Z6W) (52) were used for the calculation of surface potential with the Generalized Born model (53) and isopotential surfaces within the Poisson–Boltzmann theoretical framework (54). The calculations performed on the apo-form of CyPD and OSCP in the ATP–synthase complex did not reveal apparent complementarity in the surface potential and isopotential curves because of the complexity and extension of OSCP in the context of ATP synthase. For CyPD, the dominant surface contribution is positive and located at a region flanking the binding site for CsA. The face of CyPD opposite to the CsA binding site shows less extended but negative potential. The overall charge at pH 7.0 of CyPD, based on the sequence (GenBank accession no. NP_005720.1, mature peptide), is strongly positive (six proton charges), and therefore, we expected that the target region on OSCP should be at negative potential. By using the software BLUUES (53), we identified the lowest potential regions on OSCP (calculations performed in the ATP–synthase complex). In particular, we considered the atoms listed in Fig. S1*C* with lowest average surface potential.

ACKNOWLEDGMENTS. We thank Anna Raffaello for advice on siRNA transfection. Professor Sir John Walker at the Medical Research Council—Mitochondrial Biology Unit in Cambridge is the source of the antisubunit b antibody and Prof. Friedrich P. Thinnes, Max-Planck-Institut für Experimentelle Medizin, Abteilung Immunchemie, Göttingen, Germany, of the VDAC1 antibodies. This work was supported by grants from Telethon, Associazione Italiana per la Ricerca sul Cancro (Italy), Ministero dell'Istruzione, dell'Università e della Ricerca, Italy, and the University of Padova, Italy and National Institutes of Health Grant 1R01GM069883.

1. Bernardi P, et al. (2006) The mitochondrial permeability transition from *in vitro* artifact to disease target. *FEBS J* 273(10):2077–2099.
2. Crompton M, Ellinger H, Costi A (1988) Inhibition by cyclosporin A of a Ca^{2+}-dependent pore in heart mitochondria activated by inorganic phosphate and oxidative stress. *Biochem J* 255(1):357–360.
3. Raaflaub J (1953) Die schwellung isolierter leberzell mitochondrien und ihre physikalisch beeinflußarkeit. *Helv Physiol Pharmacol Acta* 11:142–156.
4. Pfeiffer DR, Kuo TH, Tchen TT (1976) Some effects of Ca^{2+}, Mg^{2+}, and Mn^{2+} on the ultrastructure, light-scattering properties, and malic enzyme activity of adrenal cortex mitochondria. *Arch Biochem Biophys* 176(2):556–563.
5. Hunter DR, Haworth RA, Southard JH (1976) Relationship between configuration, function, and permeability in calcium-treated mitochondria. *J Biol Chem* 251(16): 5069–5077.
6. Hunter DR, Haworth RA (1979) The Ca^{2+}-induced membrane transition in mitochondria. I. The protective mechanisms. *Arch Biochem Biophys* 195(2):453–459.
7. Haworth RA, Hunter DR (1979) The Ca^{2+}-induced membrane transition in mitochondria. II. Nature of the Ca^{2+} trigger site. *Arch Biochem Biophys* 195(2):460–467.
8. Hunter DR, Haworth RA (1979) The Ca^{2+}-induced membrane transition in mitochondria. III. Transitional Ca^{2+} release. *Arch Biochem Biophys* 195(2):468–477.
9. Kinnally KW, Campo ML, Tedeschi H (1989) Mitochondrial channel activity studied by patch-clamping mitoplasts. *J Bioenerg Biomembr* 21(4):497–506.
10. Petronilli V, Szabò I, Zoratti M (1989) The inner mitochondrial membrane contains ion-conducting channels similar to those found in bacteria. *FEBS Lett* 259(1):137–143.
11. Szabó I, Zoratti M (1991) The giant channel of the inner mitochondrial membrane is inhibited by cyclosporin A. *J Biol Chem* 266(6):3376–3379.
12. Szabó I, Bernardi P, Zoratti M (1992) Modulation of the mitochondrial megachannel by divalent cations and protons. *J Biol Chem* 267(5):2940–2946.
13. Griffiths EJ, Halestrap AP (1993) Protection by Cyclosporin A of ischemia/reperfusion-induced damage in isolated rat hearts. *J Mol Cell Cardiol* 25(12):1461–1469.
14. Palma E, et al. (2009) Genetic ablation of cyclophilin D rescues mitochondrial defects and prevents muscle apoptosis in collagen VI myopathic mice. *Hum Mol Genet* 18(11): 2024–2031.
15. Beutner G, Rück A, Riede B, Welte W, Brdiczka D (1996) Complexes between kinases, mitochondrial porin and adenylate translocator in rat brain resemble the permeability transition pore. *FEBS Lett* 396(2-3):189–195.
16. Kokoszka JE, et al. (2004) The ADP/ATP translocator is not essential for the mitochondrial permeability transition pore. *Nature* 427(6973):461–465.
17. Krauskopf A, Eriksson O, Craigen WJ, Forte MA, Bernardi P (2006) Properties of the permeability transition in *VDAC1*$^{-/-}$ mitochondria. *Biochim Biophys Acta* 1757(5-6): 590–595.
18. Baines CP, Kaiser RA, Sheiko T, Craigen WJ, Molkentin JD (2007) Voltage-dependent anion channels are dispensable for mitochondrial-dependent cell death. *Nat Cell Biol* 9(5):550–555.
19. Baines CP, et al. (2005) Loss of cyclophilin D reveals a critical role for mitochondrial permeability transition in cell death. *Nature* 434(7033):658–662.
20. Basso E, et al. (2005) Properties of the permeability transition pore in mitochondria devoid of Cyclophilin D. *J Biol Chem* 280(19):18558–18561.
21. Nakagawa T, et al. (2005) Cyclophilin D-dependent mitochondrial permeability transition regulates some necrotic but not apoptotic cell death. *Nature* 434(7033):652–658.
22. Schinzel AC, et al. (2005) Cyclophilin D is a component of mitochondrial permeability transition and mediates neuronal cell death after focal cerebral ischemia. *Proc Natl Acad Sci USA* 102(34):12005–12010.
23. De Marchi U, Basso E, Szabò I, Zoratti M (2006) Electrophysiological characterization of the Cyclophilin D-deleted mitochondrial permeability transition pore. *Mol Membr Biol* 23(6):521–530.
24. Giorgio V, et al. (2009) Cyclophilin D modulates mitochondrial F_0F_1-ATP synthase by interacting with the lateral stalk of the complex. *J Biol Chem* 284(49):33982–33988.
25. Rees DM, Leslie AG, Walker JE (2009) The structure of the membrane extrinsic region of bovine ATP synthase. *Proc Natl Acad Sci USA* 106(51):21597–21601.
26. Giorgio V, et al. (2012) The effects of idebenone on mitochondrial bioenergetics. *Biochim Biophys Acta* 1817(2):363–369.
27. Johnson KM, et al. (2005) Identification and validation of the mitochondrial F1F0-ATPase as the molecular target of the immunomodulatory benzodiazepine Bz-423. *Chem Biol* 12(4):485–496.
28. Stelzer AC, et al. (2010) NMR studies of an immunomodulatory benzodiazepine binding to its molecular target on the mitochondrial F1F0-ATPase. *Biopolymers* 93(1): 85–92.
29. Gledhill JR, Montgomery MG, Leslie AG, Walker JE (2007) Mechanism of inhibition of bovine F1-ATPase by resveratrol and related polyphenols. *Proc Natl Acad Sci USA* 104(34):13632–13637.
30. Adachi K, et al. (2007) Coupling of rotation and catalysis in F1-ATPase revealed by single-molecule imaging and manipulation. *Cell* 130(2):309–321.
31. Wittig I, Schägger H (2008) Structural organization of mitochondrial ATP synthase. *Biochim Biophys Acta* 1777(7-8):592–598.
32. Tomasetig L, Di Pancrazio F, Harris DA, Mavelli I, Lippe G (2002) Dimerization of F0F1ATP synthase from bovine heart is independent from the binding of the inhibitor protein IF1. *Biochim Biophys Acta* 1556(2-3):133–141.
33. Garrett NE, Penefsky HS (1975) Physical and enzymatic properties of nucleotide-depleted beef heart mitochondrial adenosine triphosphatase. *J Supramol Struct* 3(5-6):469–478.
34. Halestrap AP (2009) What is the mitochondrial permeability transition pore? *J Mol Cell Cardiol* 46(6):821–831.
35. Brustovetsky N, Klingenberg M (1996) Mitochondrial ADP/ATP carrier can be reversibly converted into a large channel by Ca^{2+}. *Biochemistry* 35(26):8483–8488.
36. Brenner C, et al. (2000) Bcl-2 and Bax regulate the channel activity of the mitochondrial adenine nucleotide translocator. *Oncogene* 19(3):329–336.
37. Brustovetsky N, Tropschug M, Heimpel S, Heidkämper D, Klingenberg M (2002) A large Ca^{2+}-dependent channel formed by recombinant ADP/ATP carrier from Neurospora crassa resembles the mitochondrial permeability transition pore. *Biochemistry* 41(39):11804–11811.
38. Herick K, Krämer R, Lühring H (1997) Patch clamp investigation into the phosphate carrier from Saccharomyces cerevisiae mitochondria. *Biochim Biophys Acta* 1321(3): 207–220.
39. Blatt NB, et al. (2002) Benzodiazepine-induced superoxide signals B cell apoptosis: Mechanistic insight and potential therapeutic utility. *J Clin Invest* 110(8):1123–1132.
40. Papageorgiou S, Melandri AB, Solaini G (1998) Relevance of divalent cations to ATP-driven proton pumping in beef heart mitochondrial F0F1-ATPase. *J Bioenerg Biomembr* 30(6):533–541.
41. Nathanson L, Gromet-Elhanan Z (2000) Mutations in the beta-subunit Thr^{159} and Glu^{184} of the *Rhodospirillum rubrum* F_0F_1 ATP synthase reveal differences in ligands for the coupled Mg^{2+}- and decoupled Ca^{2+}-dependent F_0F_1 activities. *J Biol Chem* 275(2):901–905.
42. Sileikyte J, et al. (2011) Regulation of the inner membrane mitochondrial permeability transition by the outer membrane translocator protein (peripheral benzodiazepine receptor). *J Biol Chem* 286(2):1046–1053.
43. Youle RJ, Narendra DP (2011) Mechanisms of mitophagy. *Nat Rev Mol Cell Biol* 12(1): 9–14.
44. Nicolli A, Basso E, Petronilli V, Wenger RM, Bernardi P (1996) Interactions of cyclophilin with the mitochondrial inner membrane and regulation of the permeability transition pore, and cyclosporin A-sensitive channel. *J Biol Chem* 271(4):2185–2192.
45. Frezza C, Cipolat S, Scorrano L (2007) Organelle isolation: Functional mitochondria from mouse liver, muscle and cultured fibroblasts. *Nat Protoc* 2(2):287–295.
46. Fontaine E, Eriksson O, Ichas F, Bernardi P (1998) Regulation of the permeability transition pore in skeletal muscle mitochondria. Modulation by electron flow through the respiratory chain complex I. *J Biol Chem* 273(20):12662–12668.
47. Di Pancrazio F, et al. (2004) In vitro and in vivo studies of F0F1ATP synthase regulation by inhibitor protein IF1 in goat heart. *Biochim Biophys Acta* 1659(1):52–62.
48. Ritov VB, et al. (1992) Alamethicin-induced pore formation in biological membranes. *Gen Physiol Biophys* 11(1):49–58.
49. Rehling P, et al. (2003) Protein insertion into the mitochondrial inner membrane by a twin-pore translocase. *Science* 299(5613):1747–1751.
50. Suhai T, Heidrich NG, Dencher NA, Seelert H (2009) Highly sensitive detection of ATPase activity in native gels. *Electrophoresis* 30(20):3622–3625.
51. Szabò I, Soddemann M, Leanza L, Zoratti M, Gulbins E (2011) Single-point mutations of a lysine residue change function of Bax and Bcl-xL expressed in Bax- and Bak-less mouse embryonic fibroblasts: Novel insights into the molecular mechanisms of Bax-induced apoptosis. *Cell Death Differ* 18(3):427–438.
52. Kajitani K, et al. (2008) Crystal structure of human cyclophilin D in complex with its inhibitor, cyclosporin A at 0.96-A resolution. *Proteins* 70(4):1635–1639.
53. Fogolari F, et al. (2012) Bluues: A program for the analysis of the electrostatic properties of proteins based on generalized Born radii. *BMC Bioinformatics* 13(Suppl 4):S18.
54. Madura JD, et al. (1995) Electrostatics and diffusion of molecules in solution: Simulations with the University of Houston Brownian Dynamics program. *Comput Phys Commun* 91(1–3):57–95.